Satellite and high spatio-temporal resolution data collected by Southern Elephant Seals allow an unprecedent 3D view of the Argentine Continental Shelf

Melina M. Martinez [1,2,3], Laura A. Ruiz-Etcheverry [1,2,3], Martín Saraceno[1,2,3], Anatole Gros-Martial [4,5,6] , Julieta Campagna[7], Baptiste Picard[6], and Christophe Guinet[6]

Melina.martinez@cima.fcen.uba.ar

1 Universidad de Buenos Aires, Facultad de Ciencias Exactas y Naturales, Departamento de Ciencias de la Atmósfera y los Océanos (DCAO). Buenos Aires, Argentina.
2 CONICET – Universidad de Buenos Aires. Centro de Investigaciones del Mar y la Atmósfera (CIMA). Buenos Aires, Argentina.
3 Instituto Franco-Argentino de Estudios sobre el Clima y sus Impactos (IFAECI) – IRL 3351 – CNRS-CONICET-IRD-UBA. Buenos Aires, Argentina.
4 ENSTA-Bretagne, UMR6285 Lab-STICC, F-29200 Brest, France.
5 University Brest, CNRS, Ifremer, IUEM, UMR6538 Geo-Ocean, F-29280 Plouzané, France
6 Centre d'Etudes Biologiques de Chizé, UMR 7372, CNRS-La Rochelle Université, 79360 Villiers en Bois, France.
7 Wildlife Conservation Society, Argentina, and Marine Programs, Amenábar 1595

1. INTRODUCTION

The Argentine Continental Shelf (ACS), which is the largest continental shelf of the southern hemisphere and one of the most productive ecosystems of the world ocean.

The hydrography of ACS, between 41°S and 43°S is analyzed, based on data collected between October 17 and 31, 2019 by sensors installed in 5 female southern elephant seals (SES).

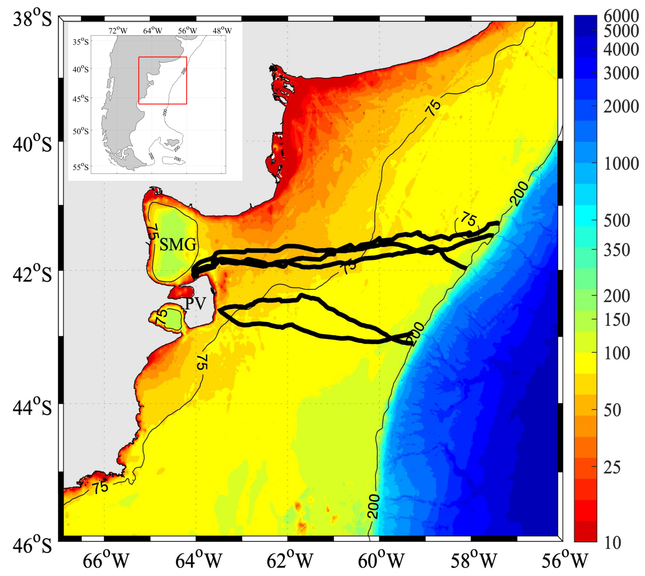

Fig 1: Trajectories from Península Valdés of 5 southern elephant seals instrumented with satellite transmitters. In colors the bathymetry (m) of the region is presented.

2. DATA

CTD (Conductivity, Temperature, and Depth) and accelerometer and hydrophone sensors attached to five elephant seals. Data are available at https://www.meop.net/database/

Wind speed at 10m from ECMWF's reanalysis model ERA5. Hourly resolution and spatial resolution of 0.25° x 0.25°. https://www.ecmwf.int/en/forecasts/dataset/ecmwf-reanalysis-v5

The tidal zonal component velocity derived from the global tidal model TPXO8 with 1/30°. https://www.tpxo.net/global/tpxo8-atlas

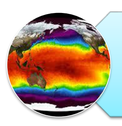

Sea Surface Temperature (SST) from Multi-scale Ultra-high Resolution L4 product (MUR - https://mur.jpl.nasa.gov/) with daily resolution and spatial resolution of 0.011° x 0.011°.

3. RESULTS AND DISCUSSION

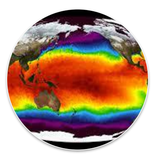

The correlation between the sea surface temperature (SST) derived from MUR and the in-situ data recorded at 15 m depth is r>0.97 for all trajectories.

The October monthly satellite images show a well-marked temperature front at the outlet of the San Matías Gulf. All northerly trajectories cross the frontal zone.

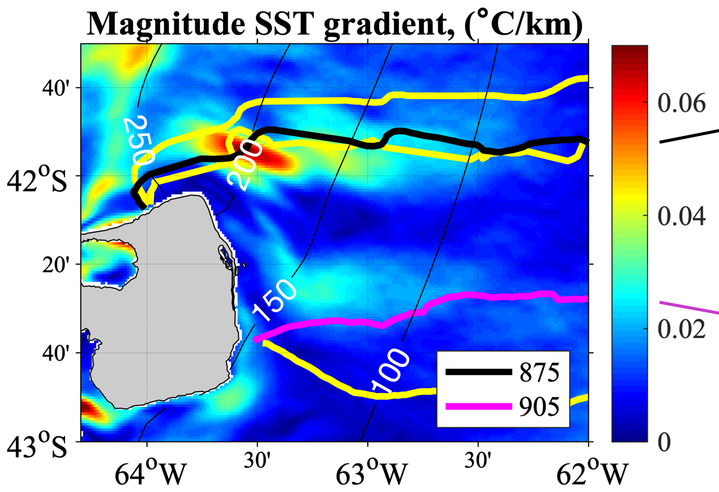

Fig. 2: Average of Sea surface temperature (SST) gradient magnitude in (ºC/km) derived from the Multi-scale Ultra-High Resolution L4 (MUR) satellite product for Octobers 2002-2019. The yellow lines represent the trajectories of SES. . Thin gray contours represent the 100, 150, 200, and 250 cm amplitude for the M2 constituent from FES2014 tide model.

The three SESs that left from the northern coast of PV crossed the region where the M2 tidal amplitude values are much greater than those along the trajectories of the SESs that left PV from the south (Fig. 2).

Time series present similar variability during the three days after departure only for the northern elephants

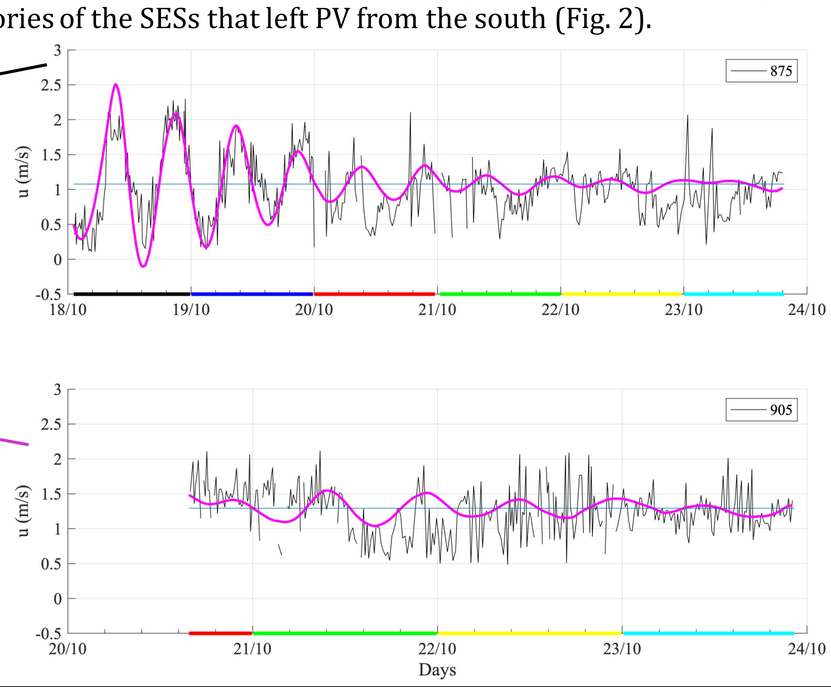

Fig. 3: Zonal component of the SESs swimming velocity (black) and the tidal current velocity derived from TPXO (magenta) along the 875 and 905 trajectories (Fig. 2). The blue line is the mean value along each trajectory of the in-situ velocity.

The vertical structure of the temperature is homogeneous from the surface to the bottom from the coast to 150 km. The vertical section displays several increases and decreases in temperature (between 10°C and 11°C) showing the presence of the front.

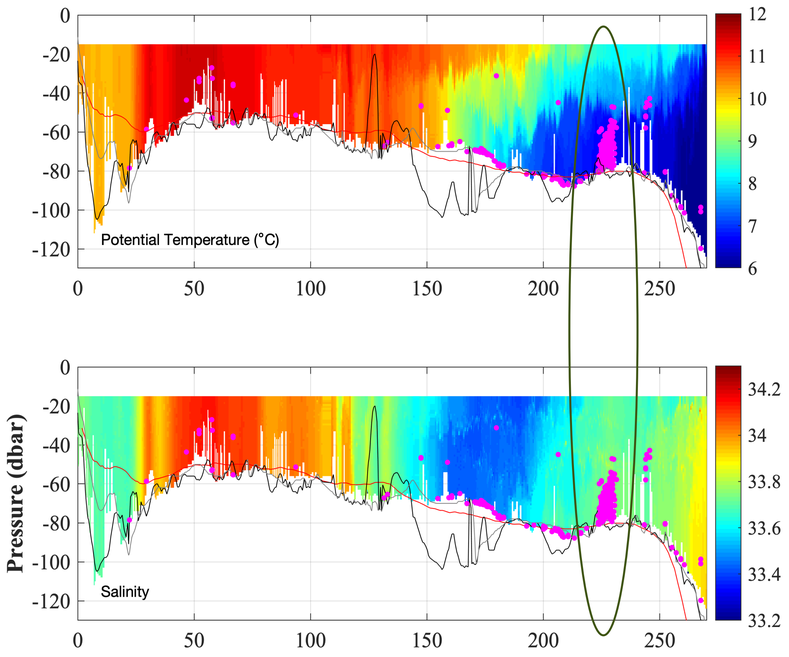

Fig 4: Profiles of potential temperature (°C, upper), salinity (middle) and sigma (kg/m^3, lower) along the trajectory SES 875. The horizontal axis is the distance in km from PV. The red, gray and black lines show the sea floor using the GEBCO-SHN 2019, GEBCO 2020 and GEBCO 2021 bathymetries respectively. Magenta dots are Prey Catch Attempts (PCA).

A large concentration of PCAs is observed between 220 and 240 km from the coast. S and T values show an increase in salinity, which coincides with a decrease in temperature of 0.5°C and an increase in density (from 26.3 to 26.4 kg/m^3). This feature is an intrusion of Malvinas water mass.

A particular event is observed in three consecutive temperature profiles of the Southern elephant. The potential temperature drop of 1°C was accompanied by an increase in salinity of ~0.2 psu (Fig. 5). There is an excellent correlation between the DTAG-4 wind estimates and ERA5 (grey and black lines). Yet, both datasets do not show an abrupt change in the wind stress intensity that explains the cooling event.

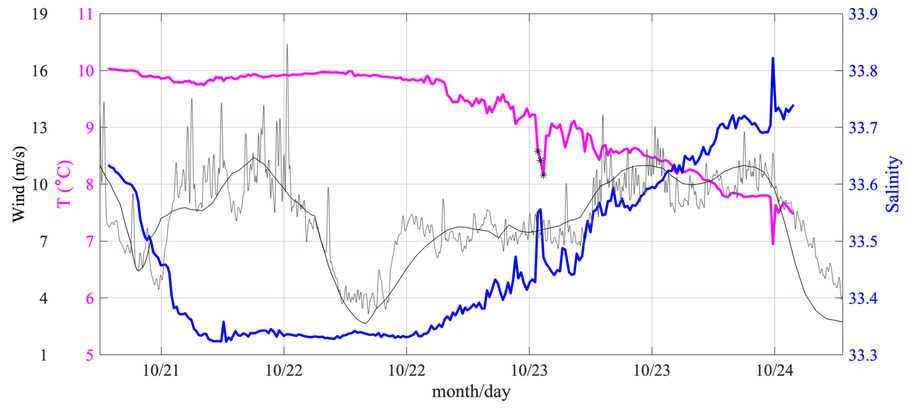

The disruption of the stratification could be due to the passage of internal waves. To be continued…

Fig. 5: In-situ temperature (magenta), salinity (blue), and wind speed from ERA5 (grey) and from DTAG-4 (black) along the 905 trajectory. DTAG-4 values were low pass filtered with a 20-minute cut-off period using a Loess filter. The black dots indicate the cooling event.

QR

Pre print MANUSCRIPT

ACKNOWLEDGMENTS

This study is a contribution to the project SABIO of EUMETSAT/CNES and PICT-2020-01468.
Martínez M. carried out this study within the framework of her doctoral thesis financed by CONICET, Argentina.

- The presence of an advective front in the northern region of PV was revealed by combining high-frequency in situ data and satellite images (Fig. 2, 4).
- SESs feed mainly between 50m and the sea bottom in the outer shelf where an intrusion of MC waters is observed (Fig. 4).
- The speed of the SES is correlated with tidal currents in the coastal portion of the northern region, in good agreement with the macro tidal regime observed (Fig. 3)
- The observed cooling event is not explained by the wind stress variation (Fig. 5)